Contributions to Geophysics and Geodesy Vol. 55/4, 2025 (419–444)

Influence of regularized derivatives in edge detectors for qualitative magnetic field interpretation – a case study from northeastern Nigeria

Ahmed Kehinde USMAN[1,2], Roland KARCOL[1], Roman PAŠTEKA[1,*]

[1] Department of Engineering Geology, Hydrogeology and Applied Geophysics, Faculty of Natural Sciences, Comenius University, Ilkovičova 6, 842 15 Bratislava, Slovakia

[2] Department of Physics, Faculty of Physical Sciences, Ahmadu Bello University, Zaria, Nigeria

Abstract: This study applies a Tikhonov regularization framework to aeromagnetic data from parts of northeastern Nigeria to enhance the resolution of magnetic anomalies and suppress geological and cultural noise. The dataset, covering twelve geological map sheets acquired by Fugro Airborne Surveys (2004–2009), was processed using a range of derivative-based edge-detection filters, including the Horizontal Gradient (HG), Analytic Signal (AS) amplitude, Tilt, Horizontal Gradient of Tilt (HG_Tilt), Theta, Normalized HG (TDX), TDXAS, Tilt Angle of the Total Horizontal Gradient (TAHG), Enhanced Tilt (ETilt), Enhanced Total Horizontal Derivative of the Tilt Angle (ETHDR), and Modified Horizontal Gradient Amplitude (MHGA). The MHGA method was further optimized by varying a constant offset (often a fraction or multiplication of π) in its computation to evaluate its sensitivity and performance. Results show that regularized derivatives effectively minimize noise amplification while preserving structural integrity, with a revisited algorithm (published by Karcol and Pašteka in year 2025) providing the most stable differentiation. The ETHDR and MHGA ($-\pi/3$) filters delineated low-magnetic anomaly zones associated with the Bima, Yolde, Pindiga, Gombe, and Kerri-Kerri Formations, indicating promising geothermal potential. High-gradient zones correspond to granitic intrusions and fault intersections that may act as heat sources and hydrothermal conduits. These results demonstrate that integrating regularized derivatives with advanced edge-detection filters significantly enhances geothermal prospectivity mapping in complex crustal settings.

Key words: Tikhonov regularization; aeromagnetic data; edge detection filters; northeastern Nigeria

*corresponding author, e-mail: roman.pasteka@uniba.sk

doi: 10.31577/congeo.2025.55.4.2

1. Introduction

Qualitative magnetic data interpretation relies heavily on edge-detection filters, which help delineate subsurface features by identifying boundaries between zones of different magnetic susceptibility. Among the most widely used techniques are the horizontal gradient (HG) method (*Cordell and Grauch, 1985*) and enhanced derivatives such as the analytic signal (*Nabighian, 1972, 1984*), tilt angle (*Miller and Singh, 1994*), and theta angle (*Wijns et al., 2005*). These techniques offer improved localization of source boundaries, but their performance can be compromised in noisy or shallow-depth environments. Consequently, modifications have been proposed to improve their stability and interpretability. The use of non-regularized derivatives in magnetic data processing, although common, often leads to noise amplification and instability, especially in areas with shallow sources or complex geology (*Oliveira et al., 2024*). Regularization techniques, such as Tikhonov regularization (*Tikhonov and Arsenin, 1977*), have been developed to address these challenges by reducing noise amplification and enhancing feature clarity. Regularized derivatives are particularly useful in stabilizing the numerical evaluation of higher-order gradients, which are inherently unstable and tend to amplify noise content (*Pašteka et al., 2009; Baniamerian et al., 2018; Melo et al., 2023; Oliveira et al., 2024; Karcol and Pašteka, 2025*). In this contribution, we present the application of a regularized derivative filter in the Fourier domain, formulated as a minimization task using classical calculus of variations, building on the framework of regularized inversion and stable numerical differentiation (*Pašteka et al., 2009; Karcol and Pašteka, 2025*). A large group of semi-automated interpretation methods use higher gradients of the interpreted field (e.g. Euler deconvolution) or methods based on analytic signal amplitude evaluation, normalized derivative methods, and many other approaches (*Nabighian, 1972, 1974, 1984; Thompson, 1982; Reid et al., 1990; Roest et al., 1992; Salem et al., 2008; Cooper and Cowan, 2006; Pašteka et al., 2009*).

In this work, we applied the Tikhonov regularization approach to the calculation of the numerical derivatives of the Total Magnetic Induction (TMI) data from part of northeastern Nigeria, aiming to enhance the resolution of magnetic anomalies while suppressing geological and cultural noise. The anomalous TMI (not reduced to the pole) and geological maps of the

area are presented in Figure 1a and 1b, respectively. The aeromagnetic data were acquired with a terrain clearance of 80 metres, a flight height of about 80 metres above ground level, and tie-line spacings of 2000 metres oriented in the NW–SE and NE–SW directions (*Oladele et al., 2022*). The TMI map represents aeromagnetic data over twelve geological map sheets—Kailatu (map sheet number 127), Madaki (map sheet number 128), Ganjuwa (map sheet number 129), Dukku (map sheet number 130), Toro (map sheet number 148), Bauchi (map sheet number 149), Alkaleri (map sheet number 150), Ako (map sheet number 151), Maijuju (map sheet number 169), Balewa (map sheet number 170), Yuli (map sheet number 171), and Futuk (map sheet number 172)—acquired by Fugro Airborne Surveys between 2004 and 2009. Each sheet covers an area of 55×55 km, giving a total study area of approximately 36,300 km^2. The TMI map reveals intensive magnetic anomalies, which usually indicate the presence of magnetite-rich rocks such as igneous intrusions, basalt flows, or metamorphic basement structures, and less intensive magnetic anomalies, which are often associated with sedimentary cover, hydrothermally altered zones or demagnetized regions caused by deep weathering (*Reeves, 2005; Nabighian et al., 2005*). The study area lies primarily within Bauchi State, with portions extending into Plateau and Gombe States. It is bounded by longitudes 9° 00′ E to 11° 00′ E and latitudes 9° 30′ N to 11° 00′ N. Geologically, the region represents a transition from the Precambrian Basement Complex to Cretaceous and Tertiary sedimentary formations, including the Bima, Yolde, Pindiga, Gombe, and

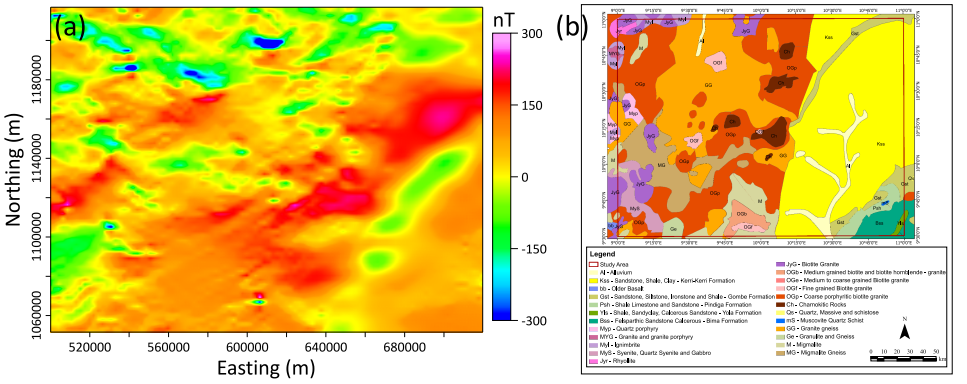

Fig. 1. (a) TMI anomaly map; (b) Geological map of part of northeastern Nigeria (*Usman and Hassan, 2025*).

Kerri-Kerri Formations, and these structures are situated in the southeastern part of the study area (*Usman and Hassan, 2025*). Structures such as intrusions and alteration zones are indicative of areas with high geothermal potential, where crustal discontinuities and radiogenic granites may act as both heat sources and hydrothermal conduits (*Salako et al., 2020*). The results for all computed edge detectors are presented in both colour and grayscale formats for detailed interpretation.

2. Non- and regularized derivatives

Traditional derivative filters—such as the horizontal gradient and vertical derivative—are known to amplify noise, particularly in near-surface regions characterized by magnetic anomalies with short wavelengths. To mitigate this limitation, we employed a Tikhonov regularization framework, which balances fidelity to the observed magnetic signal with smoothness constraints on the solution. Specifically, we adopted the C-norm approach described by *Tikhonov and Glasko (1965)* and *Pašteka et al. (2009)*, wherein the norm of the difference between adjacent solutions (corresponding to successive regularization parameters values) is plotted as a function of regularization parameter. This method assists in determining the optimal regularization parameter.

We utilized first *Pašteka et al. (2009)* (so-called original form – OF approach) and then *Karcol and Pašteka (2025)* (so-called general form – GF approach) MATLAB scripts to compute and compare the non-regularized and regularized derivatives of the magnetic field data. Regularized horizontal and vertical derivatives of the magnetic field were computed, and Fig. 2 (a, b, and c) presents the vertical derivatives for both the non-regularized and regularized solutions. The regularized derivatives computed using the *Pašteka et al. (2009)* and *Karcol and Pašteka (2025)* algorithms (Fig. 2) demonstrate the significant benefits of Tikhonov regularization in magnetic field differentiation. The non-regularized derivatives exhibit strong noise amplification (Fig. 2a), particularly over shallow and complex geological zones. The OF approach introduces smoother gradients but slightly attenuates anomaly contrast. The GF approach however achieves superior noise suppression while maintaining sharper anomaly boundaries, indicating optimal control of the trade-off between data fidelity and model smoothness

(visible in Fig. 2d). This result validates the application of regularized differentiation for stable edge enhancement in aeromagnetic dataset. Figure 3 presents the C-norm plots for first horizontal (x, y) and vertical (z) derivatives.

Consequently, the *Karcol and Pašteka (2025)* (GF approach) approach was adopted in this study to compute the following edge detectors.

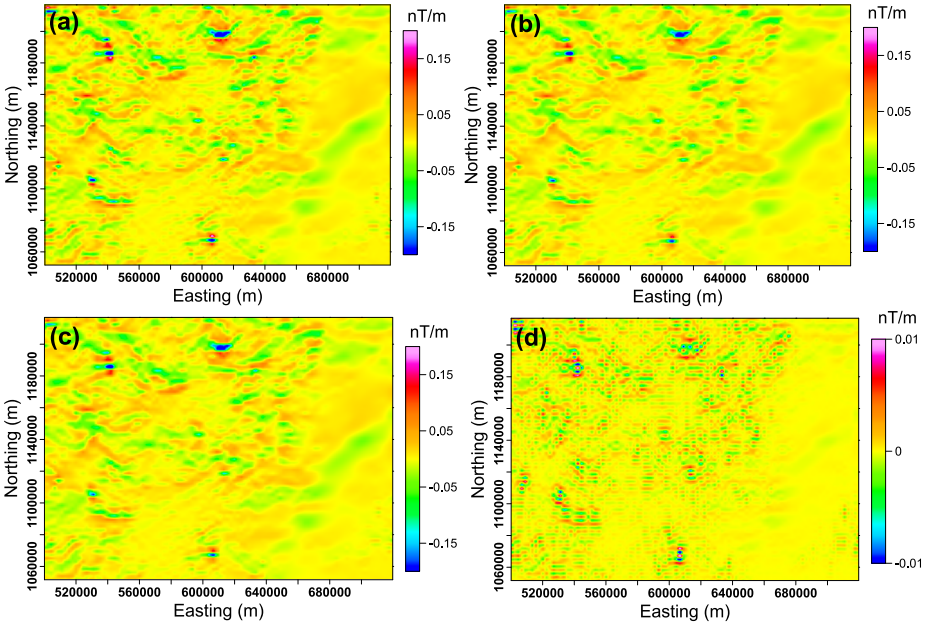

Fig. 2. First (z) derivative dT_z: (a) Non-regularized, (b) Regularized derivative using *Pašteka et al. (2009)* script (OF approach); (c) Regularized derivative using *Karcol and Pašteka (2025)* script (GF approach); (d) Difference between b) and c) solutions.

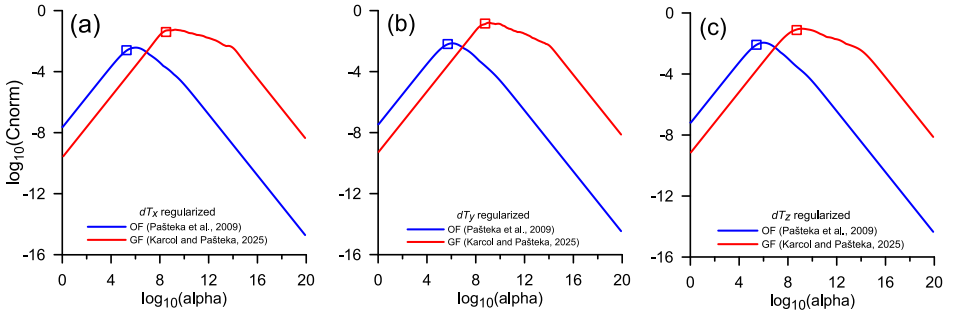

Fig. 3. Regularized derivates C-norms for: (a) x-derivate, (b) y-derivate, (c) z-derivate.

3. Edge detectors

Numerous methodologies have been developed for extracting the boundaries of buried sources, most of which rely on directional derivatives of potential field anomalies (*Núñez-Demarco et al., 2022*). *Cordell and Grauch (1985)* introduced the horizontal gradient amplitude (HG) method to delineate horizontal boundaries of subsurface structures. The HG approach, when applied to reduced-to-pole (RTP) magnetic or gravity fields, can be expressed as:

$$\mathrm{HG} = \sqrt{\left(\frac{\partial f}{\partial x}\right)^2 + \left(\frac{\partial f}{\partial y}\right)^2}, \tag{1}$$

where $\frac{\partial f}{\partial x}$ and $\frac{\partial f}{\partial y}$ represent the first-order horizontal derivatives of the potential field data function $f(x, y, z)$. *Roest et al. (1992)* introduced the analytic signal amplitude (AS), also known as the total gradient, and demonstrated that its maximum values effectively indicate the edges of buried sources with larger dimensions. The AS amplitude is expressed as follows:

$$\mathrm{AS} = \sqrt{\left(\frac{\partial f}{\partial x}\right)^2 + \left(\frac{\partial f}{\partial y}\right)^2 + \left(\frac{\partial f}{\partial z}\right)^2}, \tag{2}$$

where $\frac{\partial f}{\partial z}$ represents the first-order vertical derivative of the potential field data function.

Miller and Singh (1994) proposed the tilt-angle filter as a structural edge detector, which was further tested by *Verduzco et al. (2004)*. The method involves computing the normalized ratio of the vertical derivative of the potential field to the horizontal gradient amplitude (HG). This approach highlights the edges of subsurface structures, with zero-values corresponding to boundary locations. The tilt angle is defined as:

$$\mathrm{Tilt} = \arctan\left(\frac{\dfrac{\partial f}{\partial z}}{\mathrm{HG}}\right). \tag{3}$$

Verduzco et al. (2004) presented an edge detector, which is the total horizontal derivative of the tilt angle (HG_Tilt). It is given by:

$$\text{HG\_Tilt} = \sqrt{\left(\frac{\partial \text{Tilt}}{\partial x}\right)^2 + \left(\frac{\partial \text{Tilt}}{\partial y}\right)^2}\,. \tag{4}$$

Wijns et al. (2005) proposed the use of the theta derivative, defined as:

$$\text{Theta} = \cos\vartheta = \frac{\text{HG}}{\text{AS}}\,. \tag{5}$$

Cooper and Cowan (2006) proposed the normalized HG (TDX) filter, which uses the normalized horizontal gradient amplitude of the potential field $f(x, y, z)$. This method produces maxima that correspond to the edges of subsurface structures. It is defined as:

$$\text{TDX} = \arctan \frac{\text{HG}}{\left|\dfrac{\partial f}{\partial z}\right|}\,. \tag{6}$$

Stampolidis and Tsokas (2012) further proposed a transformation method that enhances potential field data by multiplying the normalized HG (TDX) with the analytic signal (AS) amplitude, resulting in improved edge detection and feature enhancement:

$$\text{TDXAS} = \text{TDX} \cdot \text{AS}\,. \tag{7}$$

To improve the effectiveness of the horizontal gradient amplitude in detecting the boundaries of causative sources, *Ferreira et al. (2013)* introduced the tilt angle of the total horizontal gradient (TAHG), which is calculated as follows:

$$\text{TAHG} = \arctan\left(\frac{\dfrac{\partial \text{HG}}{\partial z}}{\sqrt{\left(\dfrac{\partial \text{HG}}{\partial x}\right)^2 + \left(\dfrac{\partial \text{HG}}{\partial y}\right)^2}}\right)\,. \tag{8}$$

Here, we must point out the fact that the partial derivative $\partial\text{HG}/\partial z$ in (8) do not present the true vertical derivative of the HG function, but a pseudoderivative, calculated in the spectral domain (*de Souza et al., 2024; Pašteka et al., 2025*).

Arisoy and Dikmen (2013) presented ETilt which is the ratio of vertical derivative to horizontal derivative of AS, expressed as:

$$\mathrm{ETilt} = \arctan\left(K\,\frac{\dfrac{\partial f}{\partial z}}{\sqrt{\left(\dfrac{\partial \mathrm{AS}}{\partial x}\right)^2 + \left(\dfrac{\partial \mathrm{AS}}{\partial y}\right)^2}}\right), \tag{9}$$

where $K = 1\Big/\sqrt{(\mathrm{d}x)^2 + (\mathrm{d}y)^2}$ ($\mathrm{d}x$ and $\mathrm{d}y$ are sampling steps in the x and y directions, respectively).

According to *Arisoy and Dikmen (2013)*, when magnetic data contain anomalies with a wide range of amplitudes, the results of the Horizontal Gradient (HG) and Analytic Signal (AS) amplitude filters are often dominated by high-amplitude anomalies, which can obscure subtler features. To address this issue, they proposed the Enhanced Total Horizontal Derivative of the Tilt Angle (ETHDR) method, in which the Enhanced Tilt (ETilt) is used as a filter to improve the detection of weak or concealed magnetic sources:

$$\mathrm{ETHDR} = \sqrt{\left(\frac{\partial \mathrm{ETilt}}{\partial x}\right)^2 + \left(\frac{\partial \mathrm{ETilt}}{\partial y}\right)^2}. \tag{10}$$

Ai et al. (2024) proposed the Modified Horizontal Gradient Amplitude (MHGA) technique, which employs an improved ratio of the first-order vertical and horizontal derivatives of the horizontal gradient amplitude. This method can be applied to both gravity and reduced-to-pole (RTP) magnetic data to enhance edge detection and delineate source boundaries more accurately. The MHGA is expressed as:

$$\mathrm{MHGA} = \frac{|R+1| - |R-1|}{2}, \tag{11}$$

where

$$R = \left(\frac{\dfrac{\partial \mathrm{HG}}{\partial z}}{\sqrt{\left(\dfrac{\partial \mathrm{HG}}{\partial x}\right)^2 + \left(\dfrac{\partial \mathrm{HG}}{\partial y}\right)^2}} - \frac{\pi}{3}\right). \tag{12}$$

Also, here we point to the fact that the derivative $\partial \mathrm{HG}/\partial z$ in (12) is a pseudoderivative.

By using the MHGA method proposed by *Ai et al. (2024)*, we introduced a ratio-based approach that enhances the edge definition of potential field anomalies by varying the constant value, subtracted in the calculation of R (in the original paper of Ai et al. the value $-\pi/3$ was used). Specifically, the R parameter in the MHGA equation was calculated using different values of the subtracted constant $-\pi$, $\pi/2$, $\pi/3$, $\pi/4$, and $\pi/5$. The resulting MHGA maps were subsequently compared to identify the parameter value that provided the best edge enhancement and anomaly delineation (more details of the analysis of the role of the subtracted constant in the R calculation can be found in the Appendix). In general, we recommend always to check various values of the mentioned constant in R calculation, when applying the MHGA operator.

4. Results and discussion

The Horizontal Gradient (HG) and Analytic Signal (AS) amplitude filters are foundational techniques in magnetic data interpretation and structural mapping. The HG maps (Figs. 4a and 5a) effectively highlight areas of strong lateral variation in the magnetic field, delineating possible subsurface contacts such as lithologic boundaries, faults, and intrusive margins. These high-gradient zones are spatially associated with heat-producing granitic bodies. The AS maps (Figs. 4b and 5b) integrate the horizontal and vertical components of the magnetic field, producing amplitude responses that are largely insensitive to the direction of magnetization. This results in a more isotropic representation of source edges. However, both HG and AS tend to be dominated by high-amplitude anomalies, causing smaller or deeper features to become masked by stronger signals—an observation consistent with *Arisoy and Dikmen (2013)*. Consequently, subtle structural boundaries linked to low magnetic anomalies remain poorly resolved in these maps.

Tilt-based filters improve upon traditional gradients by normalizing vertical derivatives against horizontal gradients, making them scale-independent and enhancing the interpretability of deep or low-amplitude sources. The Tilt and Normalized Tilt (HG_Tilt) maps (Figs. 4c–d and 5c–d) partially delineate low-magnetic anomaly edges but exhibit strong noise amplification. The high-frequency content dominates, reducing clarity around ma-

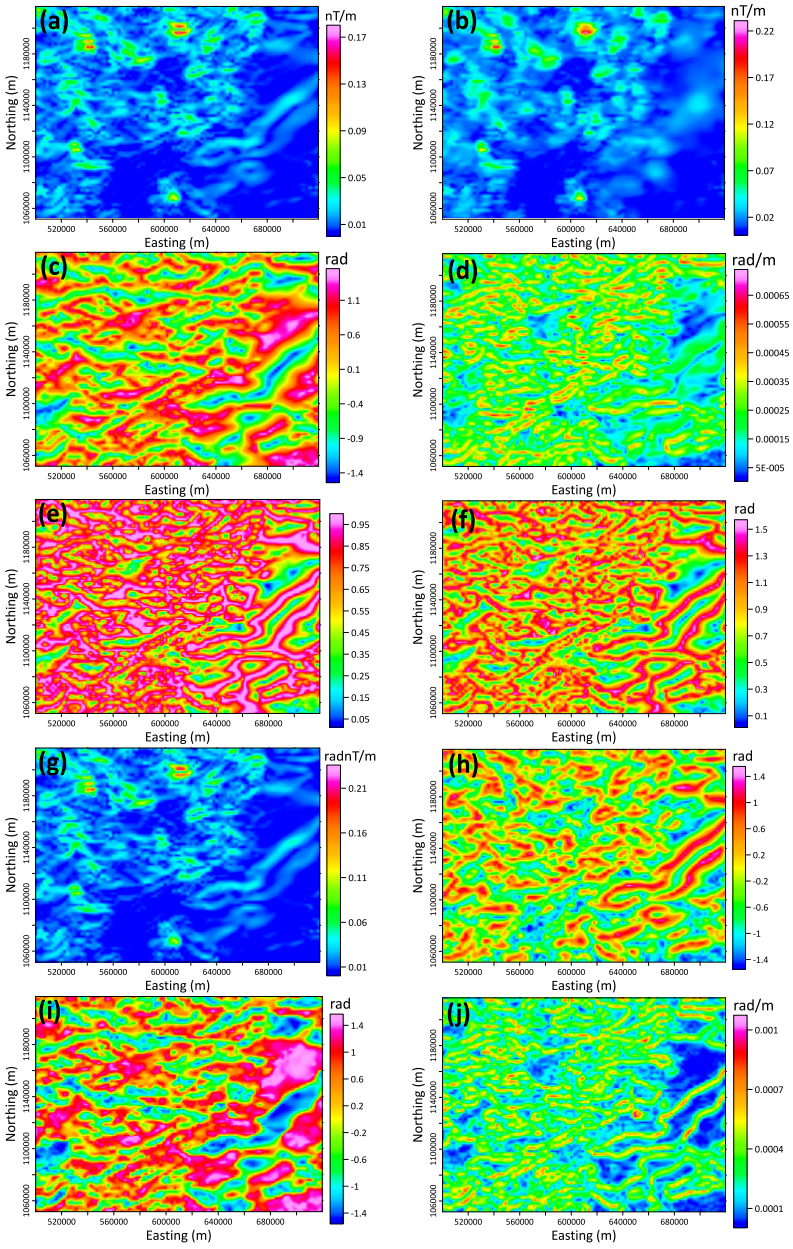

Fig. 4. Maps with colour-scale of: (a) HG, (b) AS, (c) Tilt, (d) HG_Tilt, (e) Theta, (f) TDX, (g) TDXAS, (h) TAHG, (i) ETilt, (j) ETHDR.

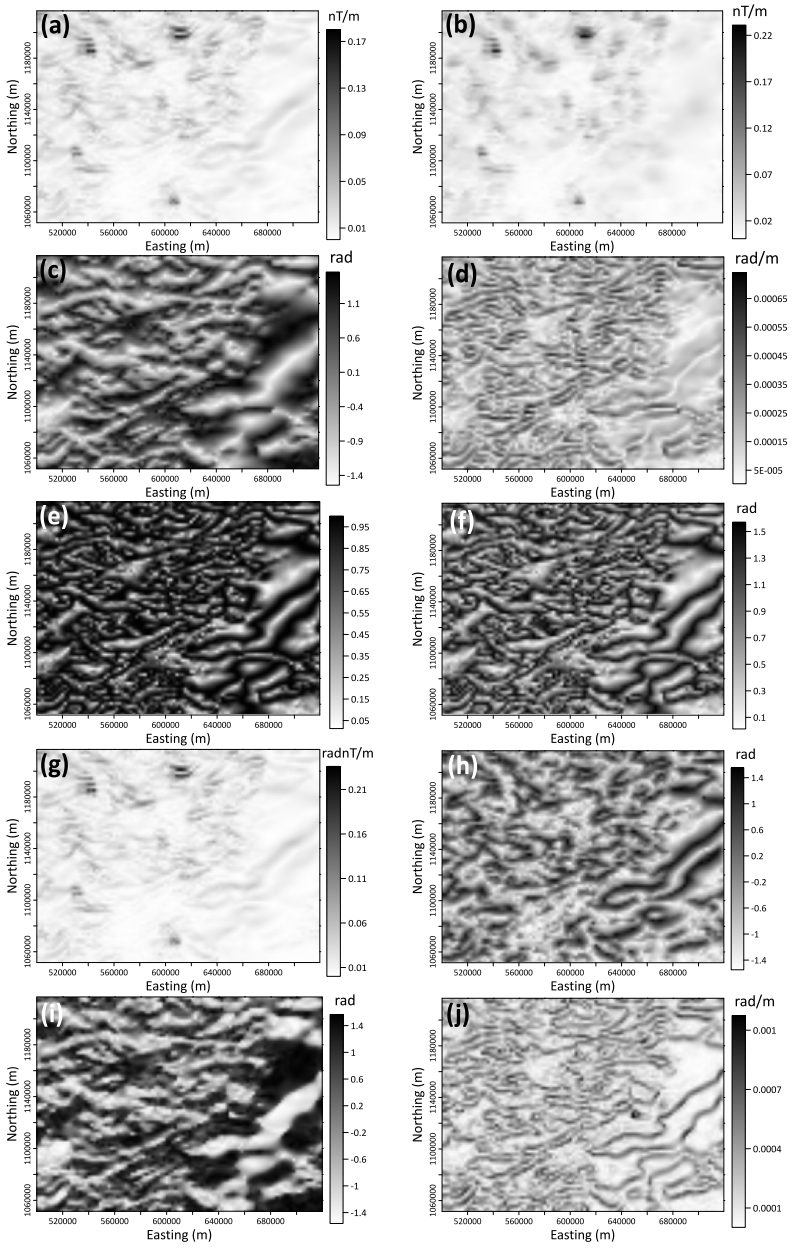

Fig. 5. Maps with grayscale of: (a) HG, (b) AS, (c) Tilt, (d) HG_Tilt, (e) Theta, (f) TDX, (g) TDXAS, (h) TAHG, (i) ETilt, (j) ETHDR.

jor anomaly sources. The Theta, TDX, TDXAS, TAHG, and ETilt maps (Figs. 4e–i and 5e–i) provide varying degrees of improvement. The TDX and TDXAS filters enhance edge detection by coupling tilt depth with analytic signal strength, enabling better visualization of shallow contacts. However, excessive enhancement introduces noise, limiting the accuracy of boundary interpretation. Among these, the Enhanced Total Horizontal Derivative of the Tilt Angle (ETHDR) (Figs. 4j and 5j) demonstrates superior performance for low-magnetic anomaly zones, such as those associated with the Bima, Yolde, Pindiga, Gombe, and Kerri-Kerri Formations. ETHDR improves the delineation of subtle features while maintaining stability, although some noise amplification persists. This behaviour confirms findings by *Arisoy and Dikmen (2013)*, where ETHDR successfully detects concealed or weak magnetic sources by mitigating the dominance of high-amplitude anomalies.

The maps in Figures 6 and 7 are the results of MHGA transformation calculated by varying the constant value, subtracted in the calculation of R. When the R parameter is computed using a constant $-\pi$, the resulting MHGA map shows no visible edges (Figs. 6a and 7a), indicating that the weighting fails to capture the magnetic contrast. Using $-\pi/2$ yields a substantial improvement—model edges corresponding to low magnetic anomalies are partially resolved, with a notable reduction in noise-to-signal amplification (Figs. 6b and 7b). Also, $-\pi/3$ yields a better substantial improvement with some clarity than $-\pi/2$ (Figs. 6c and 7c). For $-\pi/4$, and $-\pi/5$, the edges become diffused, and noise is more pronounced, lead-

Table 1. Summary of Comparative Filter Performance.

Method	**Strengths**	**Weaknesses**	**Interpretive Value**
regularized derivatives	enhanced stability, noise reduction	requires optimal parameter tuning	improves quantitative differentiation
HG/AS	good for major structures; strong anomaly localization	dominated by high amplitudes; poor subtle feature detection	first-pass mapping
Tilt/HG_Tilt	enhances weak signals	high noise sensitivity	moderate delineation
ETHDR	good detection of low anomalies; stable	slight noise amplification	good for geothermal zones
MHGA	clear detection of low anomalies; stable	slight noise amplification	excellent for geothermal zones

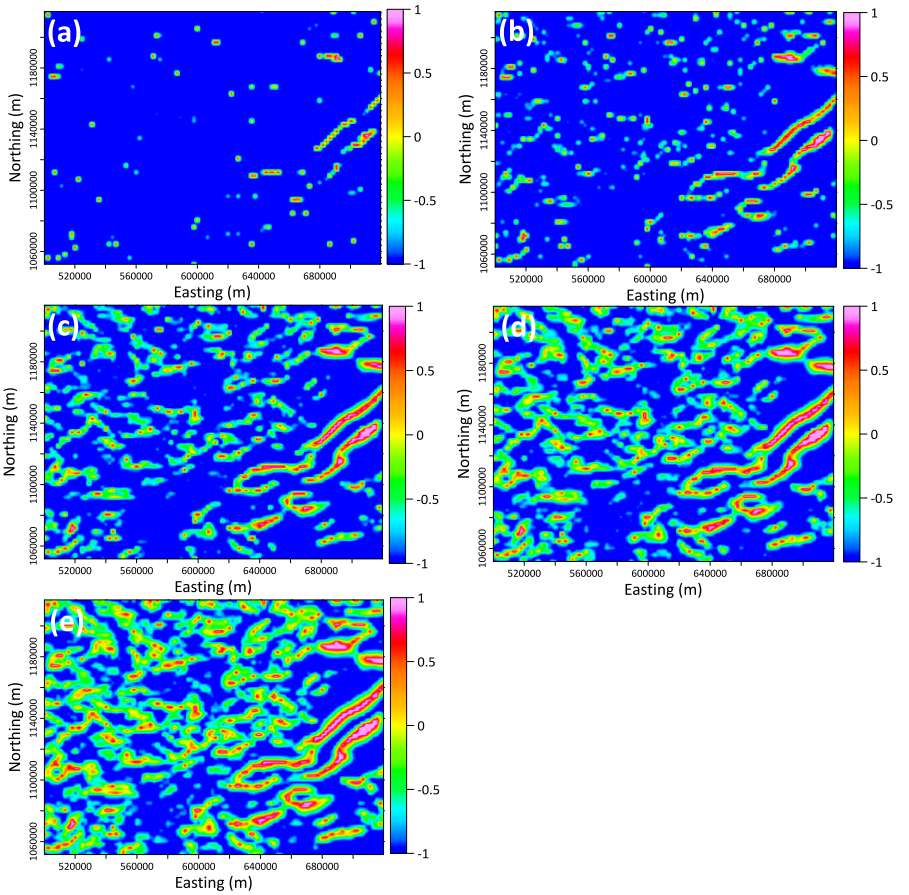

Fig. 6. MHGA colour maps for the estimated parameter R with different values of the subtracting constant: (a) π only, (b) $\pi/2$, (c) $\pi/3$, (d) $\pi/4$, (e) $\pi/5$.

ing to poor delineation of anomaly boundaries (Figs. 6d–e and 7d–e). The $-\pi/3$ configuration thus provides the most balanced outcome—achieving enhanced boundary visibility without excessive smoothing or noise amplification. This suggests that $-\pi/3$ offers an optimal trade-off between sensitivity and stability in MHGA-based edge detection, though the edges remain not perfectly delineated. At this point, we would like to point out that the above constant should be changed and tested for each processed dataset separately (more information on this topic can be found in the Appendix). Figure 8 shows MHGA ($-\pi/3$) map with delineated formations highlighted.

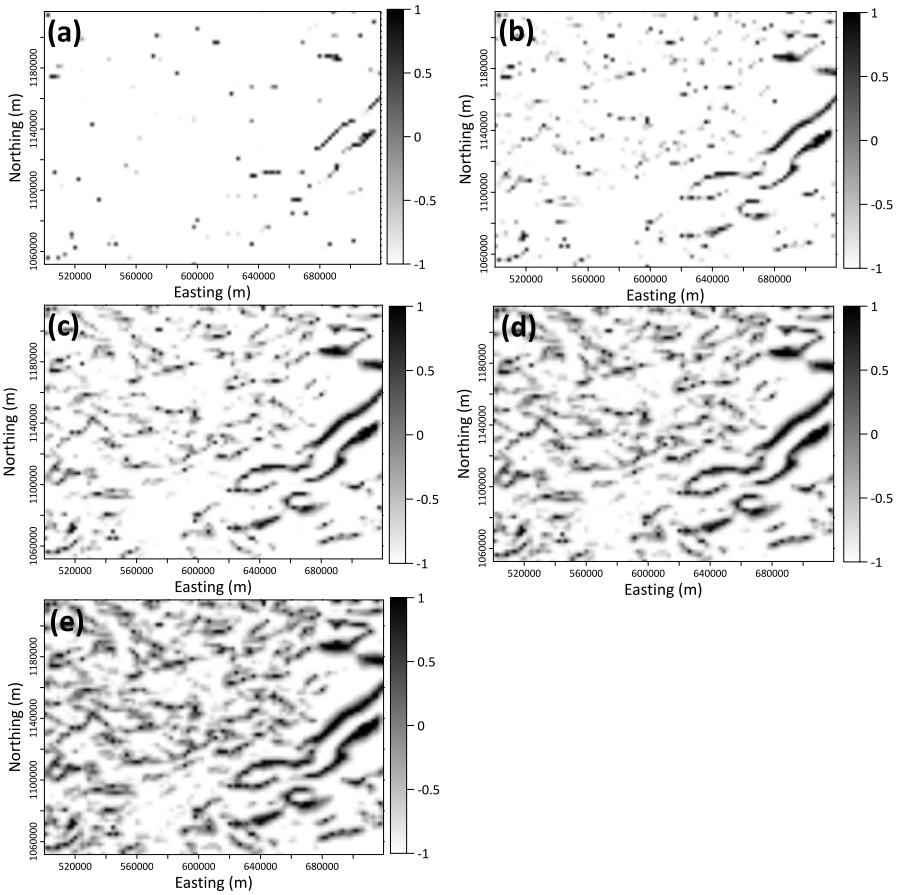

Fig. 7. MHGA grayscale maps for the estimated parameter R with different values of the subtracting constant: (a) π only, (b) $\pi/2$, (c) $\pi/3$, (d) $\pi/4$, (e) $\pi/5$.

The summary of performance of the all comparative filter is presented in Table 1.

5. Conclusion

This study employed Tikhonov regularization in combination with a suite of edge-detection filters to improve the interpretation of aeromagnetic data from northeastern Nigeria. The regularized derivatives, particularly those derived using the *Karcol and Pašteka (2025)* approach, effectively sup-

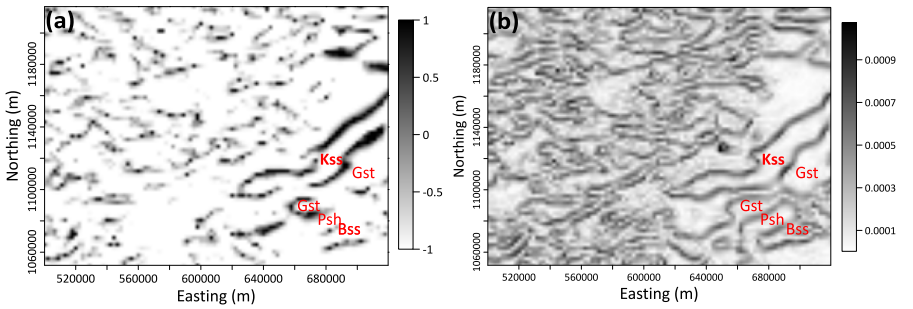

Fig. 8. Maps of MHGA ($-\pi/3$) (a) and ETHDR, (b) showing (i) Bss – Bima (ii) Psh – Pindiga (iii) Gst – Gombe (iv) Kss – Kerri-Kerri formations (note that Yolde/Yola formation overlies the Bima formation as in Fig. 1b).

pressed noise while enhancing the resolution of geological features. Among all the edge detectors evaluated, the ETHDR filter yielded the most reliable structural delineations, clearly defining low-magnetic anomaly zones linked to key lithologic units such as the Bima, Yolde, Pindiga, Gombe, and Kerri-Kerri Formations (Fig. 10). The MHGA filter, with its $-\pi/3$ parameter configuration, achieved the best balance between edge sharpness and noise stability, outperforming other parameter values. The integration of these methods demonstrates the advantages of combining regularization techniques with derivative-based edge detection to produce stable and geologically meaningful results. The identified structures—faults, intrusions, and alteration zones—are indicative of areas with high geothermal potential, where crustal discontinuities and radiogenic granites may act as both heat sources and hydrothermal conduits. From the methodical aspect, we recommend testing several values of the used constant in the R function calculation when using the MHGA method.

Acknowledgements. The authors acknowledge the support of the scientific projects VEGA 1/0587/24 and VEGA 1/0107/23. The authors are thankful for valuable comments and suggestions, resulting from the review of the original version of the submitted manuscript.

References

Ai H., Deniz Toktay H., Alvandi A., Pašteka R., Su K., Liu Q., 2024: Advancing potential field data analysis: The Modified Horizontal Gradient Amplitude method (MHGA). Contrib. Geophys. Geod., **54**, 2, 119–143, doi: 10.31577/congeo.2024.54.2.1.

Arisoy M. Ö., Dikmen Ü., 2013: Edge detection of magnetic sources using enhanced total horizontal derivative of the tilt angle. Yerbilimleri, **34**, 1, 73–82.

Baniamerian J., Liu S., Abbas M. A., 2018: Stable computation of the vertical gradient of potential field data based on incorporating the smoothing filters. Pure Appl. Geophys., **175**, 8, 2785–2806, doi: 10.1007/s00024-018-1857-2.

Cooper G. R. J., Cowan D. R., 2006: Enhancing potential field data using filters based on the local phase. Comput. Geosci., **32**, 10, 1585–1591, doi: 10.1016/j.cageo.2006.02.016.

Cordell L., Grauch V. J. S., 1985: Mapping basement magnetization zones from aeromagnetic data in the San Juan Basin. In: Hinze W. J., Kane M. F., O'Hara N. W., Reford M. S., Tanner J., Weber C. (Eds.): The Utility of Regional Gravity and Magnetic Anomaly Maps. SEG Publication, New Mexico, pp. 181–197, doi: 10.1190/1.0931830346.ch16.

de Souza J., Oliveira S. P., Szameitat L. S. A., de Souza Filho O. A., Ferreira F. J. F., 2024: Fourier domain vertical derivative of the non-potential squared analytical signal of dike and step magnetic anomalies: A case of serendipity. Geophysics, **89**, 2, G1–G12, doi: 10.1190/geo2022-0760.1.

Ferreira F. J. F., de Souza J., Bongiolo A. B. S., Castro L. G., 2013: Enhancement of the total horizontal gradient of magnetic anomalies using the tilt angle. Geophysics, **78**, 3, J33–J41, doi: 10.1190/geo2011-0441.1.

Karcol R., Pašteka R., 2025: Regularized derivatives – Revisited. Geophysics, **90**, 3, G73–G84, doi: 10.1190/GEO2023-0787.1.

LaFehr T. R., Nabighian M. N., 2012: Fundamentals of Gravity Exploration. SEG Tulsa, 209 p.

Melo J. A., Mendonça C. A., Marangoni Y. R., 2023: Python programs to apply regularized derivatives in the magnetic tilt derivative and gradient intensity data processing: A graphical procedure to choose the regularization parameter. Appl. Comput. Geosci., **19**, 100129, doi: 10.1016/j.acags.2023.100129.

Miller H. G., Singh V., 1994: Potential field tilt – a new concept for location of potential field sources. J. Appl. Geophys., **32**, 2-3, 213–217, doi: 10.1016/0926-9851(94)90022-1.

Nabighian M. N., 1972: The analytic signal of two-dimensional magnetic bodies with polygonal cross-section; Its properties and use for automated anomaly interpretation. Geophysics, **37**, 3, 507–517, doi: 10.1190/1.1440276.

Nabighian M. N., 1974: Additional comments on the analytic signal of two-dimensional magnetic bodies with polygonal cross-section. Geophysics, **39**, 1, 85–92, doi: 10.1190/1.1440416.

Nabighian M. N., 1984: Toward a three-dimensional automatic interpretation of potential field data via generalized Hilbert transforms; fundamental relations. Geophysics, **49**, 6, 780–786, doi: 10.1190/1.1441706.

Nabighian M. N., Grauch V. J. S., Hansen R. O., LaFehr T. R., Li Y., Peirce J. W., Phillips J. D., Ruder M. E., 2005: 75th Anniversary: The historical development of the magnetic method in exploration. Geophysics, **70**, 6, 33ND–61ND, doi: 10.1190/1.2133784.

Núñez-Demarco P., Bonilla A., Sánchez-Bettucci L., Prezzi C., 2022: Potential-Field Filters for Gravity and Magnetic Interpretation: A Review. Surv. Geophys., **44**, 3, 603–664, doi: 10.1007/s10712-022-09752-x.

Oladele S., Ayolabi E. A., Olobaniyi S. B., Dublin-Green C. O., 2022: Investigation of geothermal potential of the Dahomey basin, Nigeria, through analysis of geomagnetic and geo-resistivity dataset. NRIAG J. Astron. Geophys., **11**, 1, 373–386, doi: 10.1080/20909977.2022.2141022.

Oliveira S. P., Pham L. T., Pašteka R., 2024: Regularization of vertical derivatives of potential field data using Morozov's discrepancy principle. Geophys. Prospect., **72**, 8, 2880–2892, doi: 10.1111/1365-2478.13534.

Pašteka R., Richter F. P., Karcol R., Brazda K., Hajach M., 2009: Regularized derivatives of potential fields and their role in semi-automated interpretation methods. Geophys. Prospect., **57**, 4, 507–516, doi: 10.1111/j.1365-2478.2008.00780.x.

Pašteka R., Karcol R., Florio G., 2025: On the calculation of vertical pseudoderivative from nonharmonic functions in gravimetry and magnetometry. Geophysics, **90**, 6, G187–G196, doi: 10.1190/geo2024-0556.1.

Reeves C. V., 2005: Aeromagnetic surveys: Principles, practice and interpretation. Geosoft, Toronto, Canada, 155 p.

Reid A. B., Allsop J. M., Granser H., Millett A. J., Somerton I. W., 1990: Magnetic interpretation in three dimensions using Euler deconvolution. Geophysics, **55**, 1, 80–91, doi: 10.1190/1.1442774.

Roest W. R., Verhoef J., Pilkington M., 1992: Magnetic interpretation using the 3-D analytic signal. Geophysics, **57**, 1, 116–125, doi: 10.1190/1.1443174.

Salako K. A., Adetona A. A., Rafiu A. A., Alhassan U. D., Aliyu A., Adewumi T., 2020: Assessment of Geothermal Potential of Parts of Middle Benue Trough, North-East Nigeria. J. Earth Space Phys., **45**, 4, 27–42, doi: 10.22059/jesphys.2019.260257.1007017.

Salem A., Williams S., Fairhead D., Smith R. Ravat D., 2008: Interpretation of magnetic data using tilt-angle derivatives. Geophysics, **73**, 1, L1–L10, doi: 10.1190/1.2799992.

Stampolidis A., Tsokas G. N., 2012: Use of edge delineating methods in interpreting magnetic archaeological prospection data. Archaeol. Prospect., **19**, 2, 123–140, doi: 10.1002/arp.1424.

Thompson D. T., 1982: EULDPH: A new technique for making computer-assisted depth estimates from magnetic data. Geophysics, **47**, 1, 31–37, doi: 10.1190/1.1441278.

Tikhonov A. N., Glasko V. B., 1965: Application of the regularization method to nonlinear problems. Zh. vychislit. matem. i matem. fiz., **5**, 463–473 (in Russian).

Tikhonov A. N., Arsenin B. J., 1977: Solutions of Ill-Posed Problems. John Wiley & Sons. New York, 258 p.

Usman A. K., Hassan Y. A., 2025: Geology of Northeastern Nigeria and Its Prospects for Geothermal Energy: A Review. Commun. Phys. Sci., **12**, 4, 1227–1236.

Verduzco B., Fairhead J. D., Green C. M., MacKenzie C., 2004: New insights into magnetic derivatives for structural mapping. Lead. Edge, **23**, 2, 116–119, doi: 10.1190/1.1651454.

Wijns C., Perez C., Kowalczyk P., 2005: Theta map: Edge detection in magnetic data. Geophysics, **70**, 4, L39–L43, doi: 10.1190/1.1988184.

Appendix – Analysis of the properties of the MHGA operator

For a better understanding of how the MHGA operator (Modified Horizontal Gradient Amplitude; *Ai et al., 2024*) works it is good to analyse its partial components and properties of the mathematical form of the MHGA operator (Eqs. (11) and (12) in the main paper).

For this kind of analysis, we have selected a simple gravity model of a thin horizontal ribbon, which is a 2D structure with a very small vertical dimension, width $2b$ and is positioned in the depth h (Fig. A1).

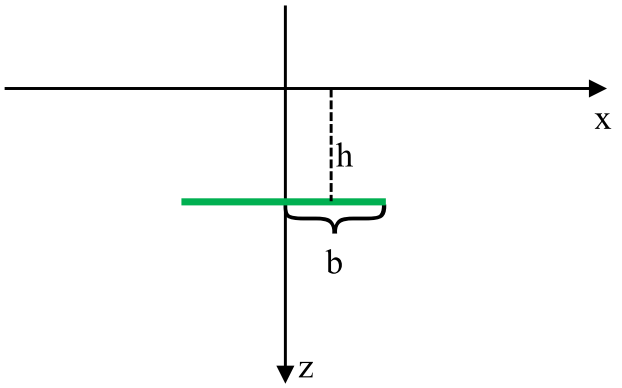

Fig. A1. Geometry of a 2D thin horizontal ribbon structure.

In the case of such an object, the gravitational effect (its vertical component), as the input function $f(x,z)$ into the MHGA operator can be expressed (e.g. *LaFehr and Nabighian, 2012; p. 30*):

$$f(x,z) = V_z(x,z) = 2\kappa\mu \left(\arctan \frac{x+b}{h-z} - \arctan \frac{x-b}{h-z} \right), \tag{A-1}$$

where μ is the so-called surface density. Since this function is independent of variable y, the quantity R (Eq. (12) from the main paper) can be expressed in the form:

$$R = \frac{\dfrac{\partial \mathrm{HGA}}{\partial z}}{\sqrt{\left(\dfrac{\partial \mathrm{HGA}}{\partial x}\right)^2 + \left(\dfrac{\partial \mathrm{HGA}}{\partial y}\right)^2}} = \frac{\dfrac{\partial}{\partial z}\left|f_x\right|}{\sqrt{\left(\dfrac{\partial}{\partial x}\left|f_x\right|\right)^2}} = \frac{\dfrac{\partial}{\partial z}\left|f_x\right|}{\left|\dfrac{\partial}{\partial x}\left|f_x\right|\right|}, \tag{A-2}$$

where:

$$\begin{aligned}
&\mathrm{HGA} = \sqrt{(f_x)^2 + (f_y)^2} = \sqrt{(f_x)^2 + 0} = |f_x|\,, \\
&f_x = \frac{\partial f}{\partial x} = \frac{\partial V_z}{\partial x} = \\
&\qquad = 2\kappa\mu\,(h-z)\left(\frac{1}{(h-z)^2 + (x+b)^2} - \frac{1}{(h-z)^2 + (x-b)^2}\right), \\
&\frac{\partial}{\partial z}\,|f_x| = \mathrm{sign}\,(f_x)\cdot 2\kappa\mu\left(\frac{1}{(h-z)^2 + (x-b)^2} - \frac{1}{(h-z)^2 + (x+b)^2} + \right. \\
&\qquad \left. + \frac{2\,(h-z)^2}{\left[(h-z)^2 + (x+b)^2\right]^2} - \frac{2\,(h-z)^2}{\left[(h-z)^2 + (x-b)^2\right]^2}\right), \\
&\left|\frac{\partial}{\partial x}\,|f_x|\right| = \left|\mathrm{sign}\,(f_x)\cdot 4\kappa\mu\,(h-z)\left(\frac{x-b}{\left[(h-z)^2 + (x-b)^2\right]^2} - \right.\right. \\
&\qquad \left.\left. - \frac{x+b}{\left[(h-z)^2 + (x+b)^2\right]^2}\right)\right|.
\end{aligned} \tag{A-3}$$

Figure A2 shows the individual fields for the set of input parameters ($b = h = 10$ m and $\mu = 5500$ kg·m^{-2}).

Here, let us focus on the images for the quantity R and for the MHGA operator itself. From the expression for R (without the constant $-\pi/3$), we can see that it must contain a singularity at points where f_x has an extreme value. This is indeed what happens here – so the amplitude of the R function depends on the size of the measurement step and thus on how close the calculation point gets to the inflection point on the input field f curve. As can be seen in Fig. A2, the R function already responds with its maxima to the specified positions of the inflection points of the original function, but only the MHGA operator (which is actually a linearly saturated function) brings it "under control" – into the useful interval [−1,+1]. At first glance, it may not seem so, but the MHGA function is only a modified part of the R function. This property becomes apparent when they are superimposed on each other (Fig. A3). Here we can see that the MHGA operator acts

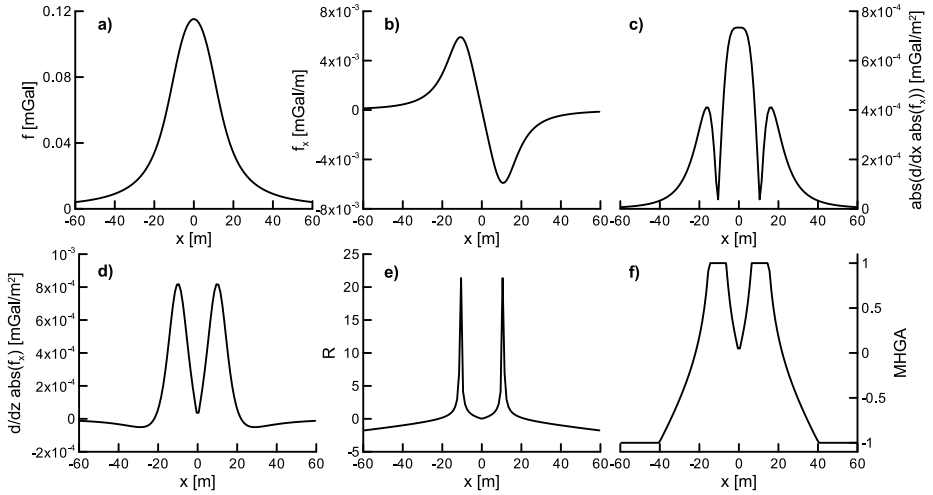

Fig. A2. Graphs of individual fields (components) from equation (A-3), function, R and operator MHGA for a model of 2D thin horizontal ribbon with parameters $b = h = 10$ m and $\mu = 5500$ kg·m^{-2}.

like a "trimmer" or "cutter" (from the word trim or prune or cut) of the function R.

This brings us to the role of the constant $-\pi/3$, in Eq. (12). When we subtract the constant from the fraction in the variable R, the result is a

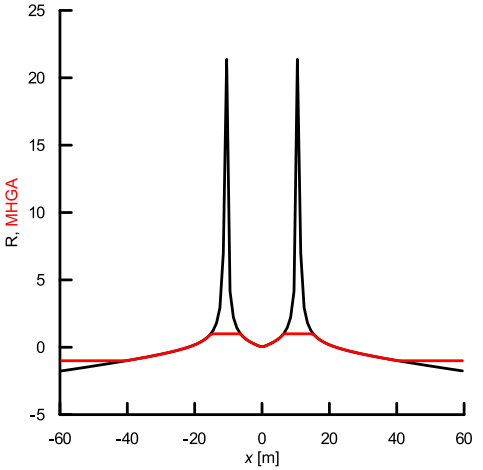

Fig. A3. Graphs of the function R and the operator MHGA for a model of 2D thin horizontal ribbon with parameters $b = h = 10$ m and $\mu = 5500$ kg·m^{-2}.

downward shift of the curve by exactly the selected constant (Fig. A4). The MHGA "trimmer" then cuts out the upper part (towards the peaks) of this shifted curve. Based on the above finding, it is possible to propose a modified form of the relationship for calculating the R function (Eq. (12) in the main text):

$$R = \left(\frac{\dfrac{\partial \mathrm{HG}}{\partial z}}{\sqrt{\left(\dfrac{\partial \mathrm{HG}}{\partial x}\right)^2 + \left(\dfrac{\partial \mathrm{HG}}{\partial y}\right)^2}} + C \right), \tag{A-4}$$

where it is appropriate to change the constant C and qualitatively assess the obtained MHGA (we usually use multiples and parts of π, with negative

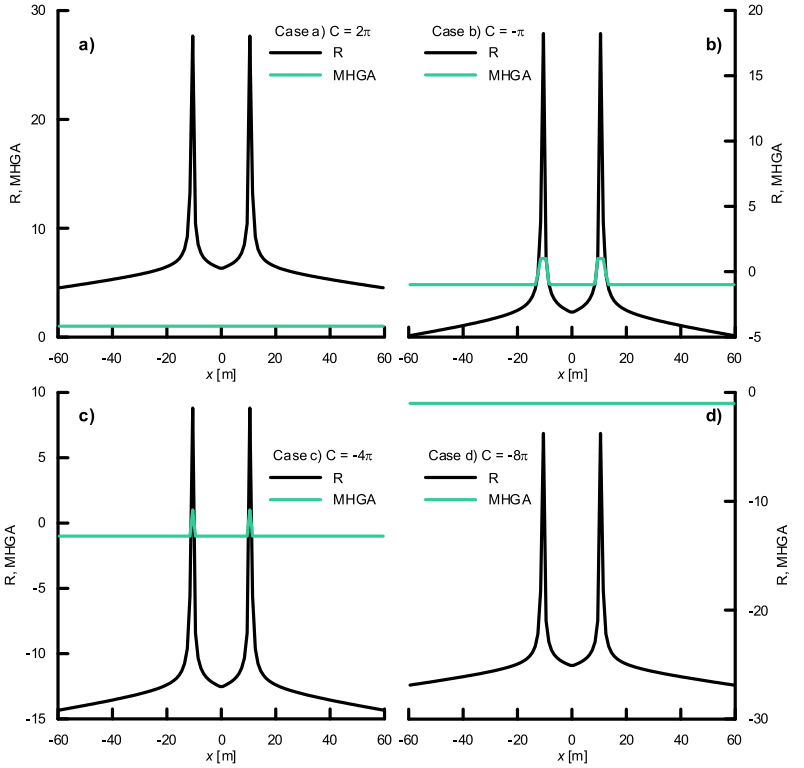

Fig. A4. Graphs of the function R and the operator MHGA for different values of the constant C (for a model of 2D thin horizontal ribbon with parameters $b = h = 10$ m and $\mu = 5500$ kg·m^{-2}).

and positive sign).

MHGA transformation is also sensitive to the size of the discretization of the interpreted anomalous field (grid cell size in the case of grids, step along the horizontal axis in the case of profile data). In Figs. A5 and A6 we can see several examples of the MHGA field for various sizes of the grid cell size and the used constant C in the Eq. (A-4) (model is composed of two rectangular prisms with horizontal dimensions 2×2 km, vertical dimension 2.5 km, depth of the upper edge 20 m and density contrast +1000 kg·m^{-3}). Graphs of R function and MHGA operator values along a central interpretation line are shown in Figs. A7 and A8. Maps in the Figs. A5 and A6 (and graphs

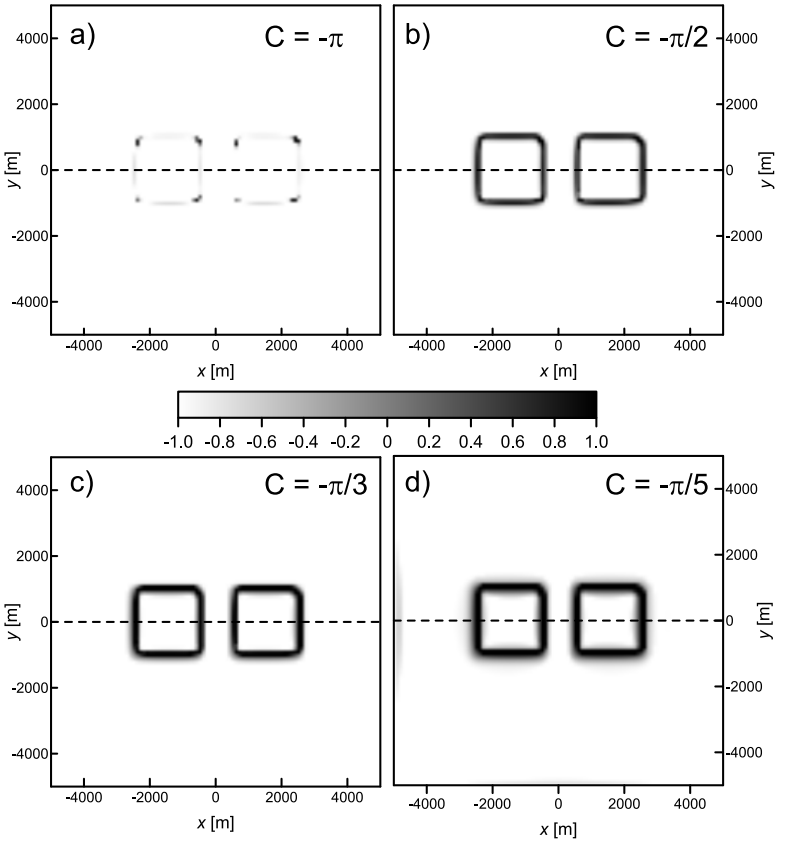

Fig. A5. Image maps of the MHGA values for different values of the constant C (for a model composed of two rectangular prisms). Used grid cell size: 100×100 m. The dashed line shows the position of the interpretation line used in Fig. A7.

in Figs. A7 and A8) clearly show how the sharpness of the prism edges in the MHGA field is affected by the used C value and the grid-cell size of the processed grid. For the case with 100×100 m grid, from all tested C values the used $-\pi/2$ gave the sharpest boundaries of prisms boundaries (Fig. A5b). For the case with 300×300 m grid all results were too blurry and it can be seen that this grid is too sparse for this kind of qualitative interpretation. The graphs in Fig. A8 clearly show that the sampling step used (300×300 m) is too coarse and that the resulting interpolation errors contribute to the insufficient determination of the positions of the prism edges (nevertheless, the MHGA operator shows very good properties here

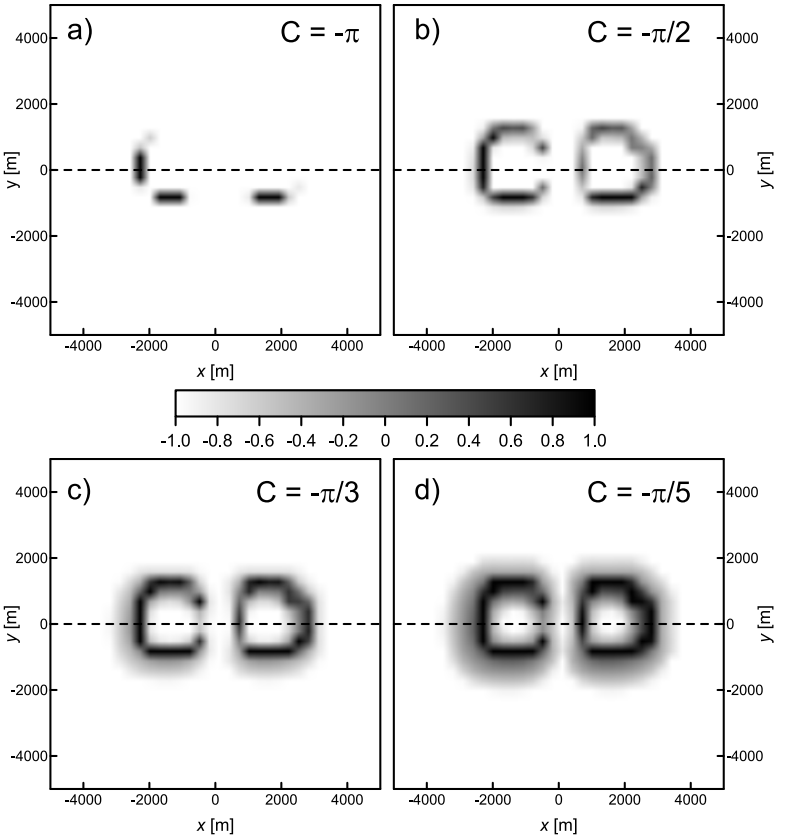

Fig. A6. Image maps of the MHGA values for different values of the constant C (for a model composed of two rectangular prisms). Used grid cell size: 300×00 m. The dashed line shows the position of the interpretation line used in Fig. A8.

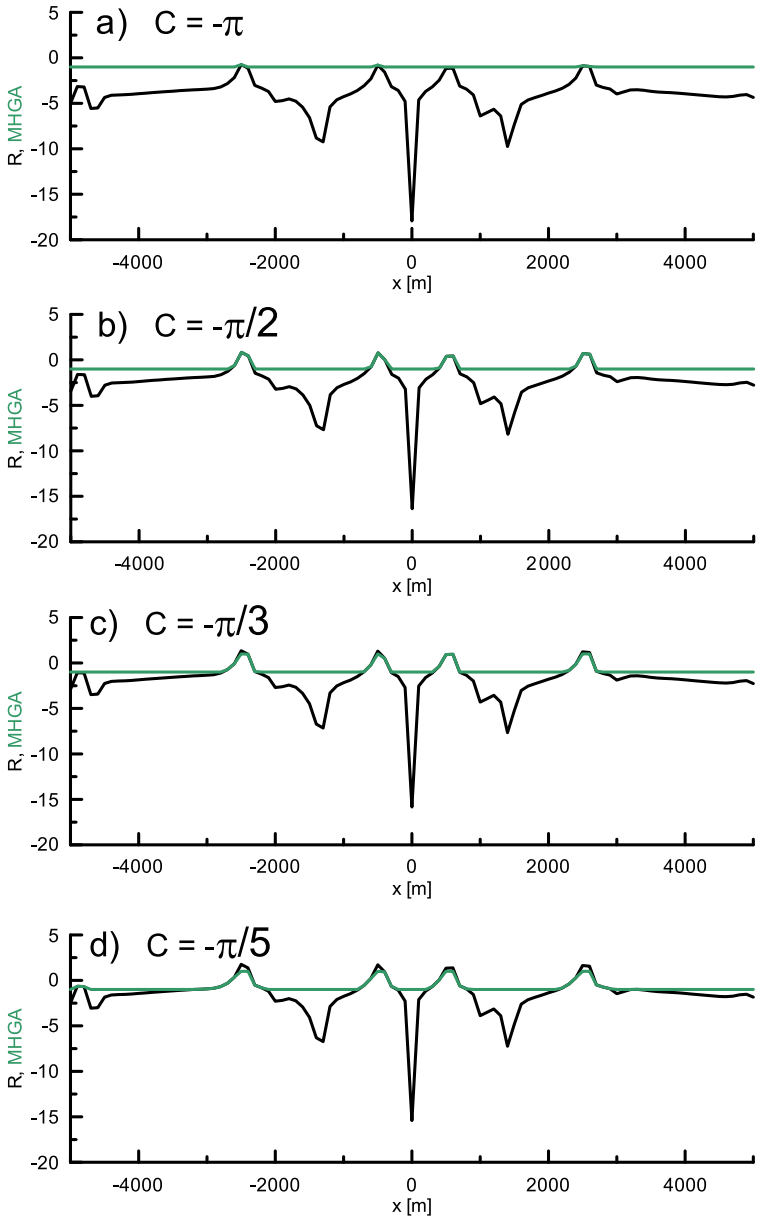

Fig. A7. Graphs of the function R (black) and the operator MHGA (green) for different values of the constant C (for a model composed of two rectangular prisms, used grid cell size: 100×100 m).

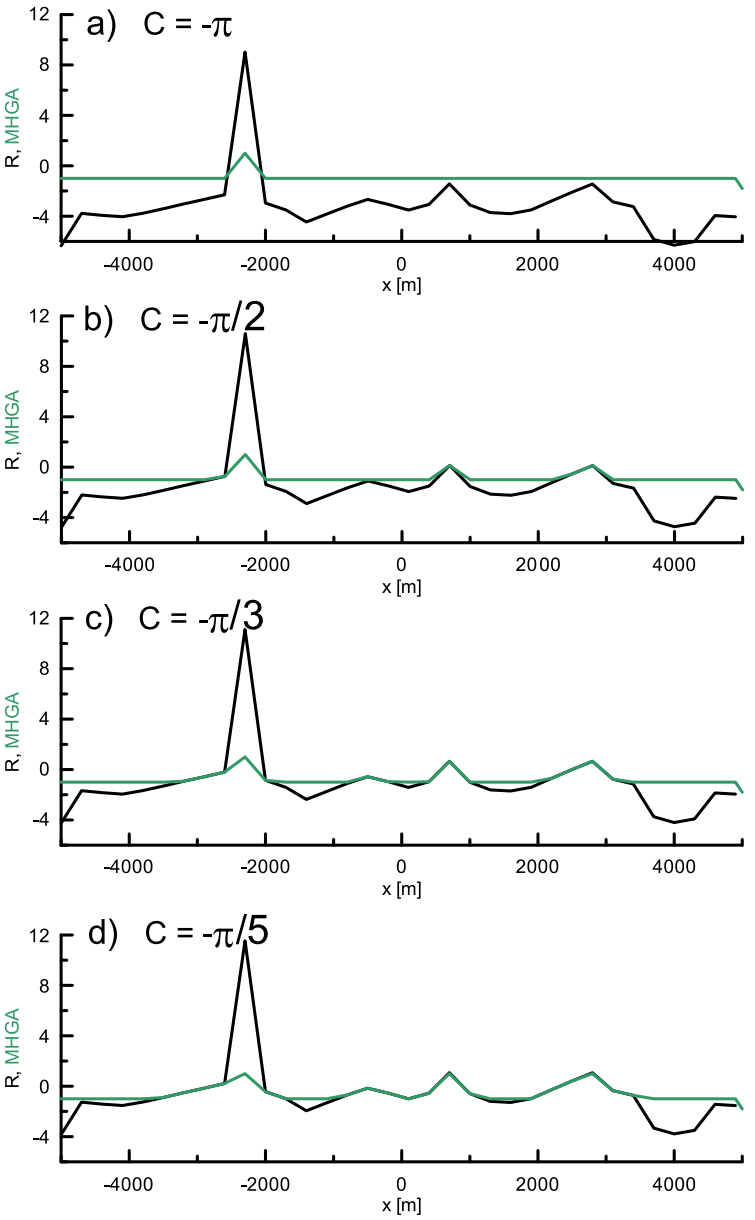

Fig. A8. Graphs of the function R (black) and the operator MHGA (green) for different values of the constant C (for a model composed of two rectangular prisms, used grid cell size: 300×300 m).

compared to the R function – the local maxima of MHGA are approximately at the same level, even in case where the R function reaches significantly higher value at $x = -2300$ m).